



# Corrosion of dental amalgams: electrochemical study of Ag–Hg, Ag–Sn and Sn–Hg phases

Heloísa A. Acciari<sup>a,b</sup>, Antonio C. Guastaldi<sup>b</sup>, Christopher M.A. Brett<sup>a,\*</sup>

<sup>a</sup> Departamento de Química, Universidade de Coimbra, 3004-535 Coimbra, Portugal

<sup>b</sup> Departamento de Físico-Química, Instituto de Química de Araraquara-UNESP, C.P. 355, Araraquara, SP, Brazil

Received 24 June 2000; received in revised form 12 January 2001

## Abstract

Dental amalgams, formed by reaction of mercury with a powder alloy containing mainly Ag, Sn, Cu and Zn, have a complex metallurgical structure which can contain up to six phases. Their observed corrosion is thus a complex process, which involves contributions from each of the phases present as well as intergranular corrosion. It is thus of interest to investigate the corrosion of individual phases present in dental amalgams. In this work the corrosion behaviour in 0.9% NaCl solution of Ag–Hg, Ag–Sn and Sn–Hg phase components of dental amalgams was investigated by electrochemical methods. The corrosion resistance was found to decrease in the order  $\gamma_1$ -Ag<sub>2</sub>Hg<sub>3</sub>,  $\gamma$ -Ag<sub>3</sub>Sn and  $\gamma_2$ -Sn<sub>7</sub>Hg. © 2001 Elsevier Science Ltd. All rights reserved.

**Keywords:** Dental amalgams; Amalgam phases; Corrosion; Electrochemical impedance

## 1. Introduction

Dental amalgam [1–3] is a metallic alloy formed by the reaction of mercury with a powder alloy containing silver (40–70%), tin (15–30%) and copper (10–30%), and sometimes also a small percentage of zinc. Products of amalgamation are the  $\gamma$ -phase of the silver–mercury system, designated  $\gamma_1$ -Ag<sub>2</sub>Hg<sub>3</sub>, the  $\gamma$ -phase of the tin–mercury system, designated  $\gamma_2$ -Sn<sub>7–8</sub>Hg, and the intermetallic compounds of the tin–copper system,  $\epsilon$ -Cu<sub>3</sub>Sn and  $\eta'$ -Cu<sub>6</sub>Sn<sub>5</sub> [2]. There are also particles of the original alloys which did not react during the amalgamation process such as, for example,  $\gamma$ -Ag<sub>3</sub>Sn and the Ag–Cu eutectic. There is thus a complex metallurgical structure, containing up to six phases, as can be seen in the micrograph of Fig. 1.

Concerns have been expressed regarding toxicity of dental amalgam, in particular with respect to marginal fracture, surface degradation, corrosion, release of corrosion products (particularly mercury) and biocompatibility.

Amalgams have been examined under different conditions similar to those encountered in the oral cavity—factors such as acidity, temperature and abrasion can all influence the corrosion rate. Mercury release has been monitored, e.g. [4,5], it being shown that a passivation layer formed on the amalgam surface reduces the release rate. Acids increase the corrosion rate and several studies varying pH have been undertaken [6,7]. Mechanical removal of amalgam residues and corrosion products, together with sharp temperature variations due to the introduction into the mouth of hot or very cold foods has also been investigated [8,9].

Direct studies of the corrosion of dental amalgams are relatively scarce. An early study [10] investigated the most appropriate formulation for imitating natural saliva. More recently, a comparative study, based only

\* Corresponding author. Tel.: +351-239-835295; fax: +351-239-835295.

E-mail address: brett@ci.uc.pt (C.M.A. Brett).

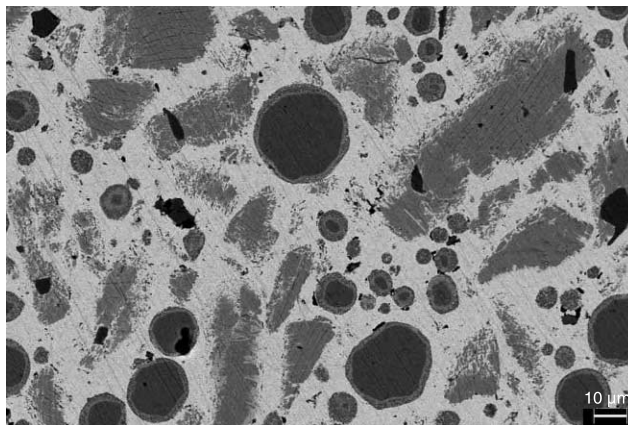


Fig. 1. Scanning electron micrograph, using backscattered electrons, of Dispersalloy dental amalgam, showing the complex multiphase structure. The large dark circular areas represent the Ag–Cu eutectic, in dark grey are Ag–Sn  $\gamma$ -phases of irregular form and different sizes, all included in a matrix of  $\gamma_1$ -Ag<sub>2</sub>Hg<sub>3</sub> in light grey.

on simple voltammetric profiles, of 16 commercial amalgams in vitro on artificial saliva showed corrosion rates varying over several orders of magnitude and a stability rating was suggested [11]. However, no attention was given to the removal of corrosion products or alteration of the surface morphology. Additionally, other electrochemical techniques now used for monitoring corrosion such as voltammetry, chronoamperometry and impedance were not employed. The usefulness of Tafel analysis and electrochemical impedance was demonstrated in a recent study comparing Dispersalloy and Velvalloy high copper dental amalgams [1].

Most research on amalgam corrosion has focused on high copper amalgams during the last 15 years. However, the great diversity of commercial amalgams, their complex metallurgical structures, the size of the microphases which can vary according to the exact mixing

conditions, the variation in the composition of natural saliva and the many variables that can affect in vitro experiments, make interpretation of the corrosion process difficult. It is thus of interest to investigate the corrosion and electrochemical behaviour of individual phases present in dental amalgams in different solutions imitating natural saliva. This information can then be correlated and used to better understand the corrosion of the amalgams which contain all these components under the various experimental conditions in the oral cavity.

In this work the corrosion of three of the phase components of dental amalgams has been investigated, in order to demonstrate the usefulness of the approach and obtain new experimental information. These were the matrix phase of the microstructure,  $\gamma_1$ -Ag<sub>2</sub>Hg<sub>3</sub>, the second most predominant phase,  $\gamma$ -Ag<sub>3</sub>Sn, and the

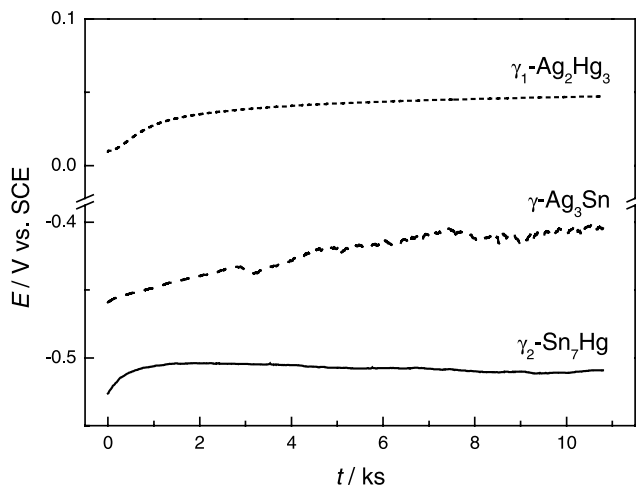


Fig. 2. Variation of open circuit potential with time during 3 h after immersion in 0.9% NaCl for the three alloys.

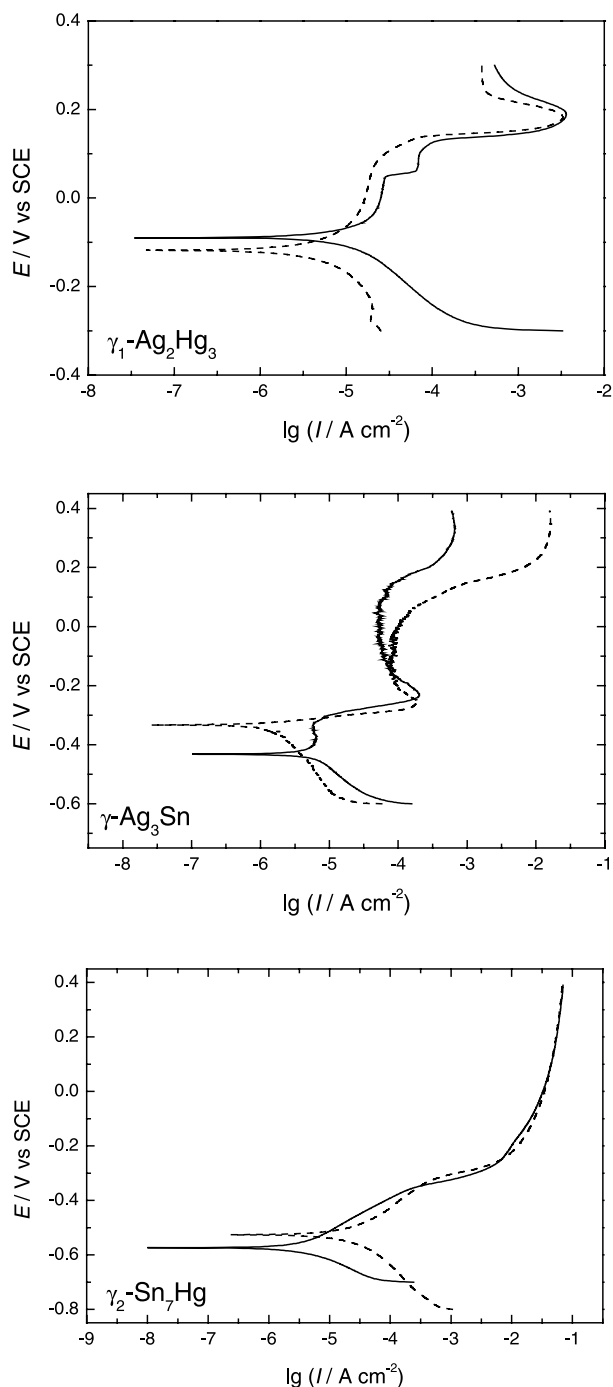


Fig. 3. Potentiodynamic polarisation curves for samples immersed for 10 min (—) and 48 h (---). Scan rate  $2.5 \text{ mV s}^{-1}$ .

phase (according to the literature [3]) most susceptible to corrosion in the oral cavity,  $\gamma_2\text{-Sn}_{7-8}\text{Hg}$ . The medium used was 0.9% aqueous sodium chloride, in order to simulate the aggressivity of the oral cavity.

## 2. Experimental

The mercury-containing alloys were made in the correct stoichiometric proportions, taking into account the phase diagrams, by mechanical amalgamation and moulding under high pressure following the criteria adopted by the American Dental Association. The Ag–Sn alloy was prepared by heating the components until they were completely melted, and then the melt was poured into a mould to form an ingot. After the ingot was completely cooled, it was heated at  $180^\circ \text{C}$  for 1 week and cooled slowly. Electrodes were made from samples by embedding in resin leaving one face exposed, area  $\sim 0.3 \text{ cm}^2$ , polishing with 600 and 1000 grade emery papers, rinsed with distilled water and dried in air. The samples were examined by scanning electron microscopy and X-ray diffraction. Important points from this analysis are that in the case of Ag–Hg there was significant residual porosity, and the Sn–Hg alloys showed evidence of the formation of tin and mercury oxides on the surface. The thickness of these oxide films is difficult to evaluate by X-ray diffraction since X-ray penetration depends on the degree of crystallinity of the film.

Electrochemical experiments were performed in a three-electrode cell containing an electrolyte similar to physiological serum (0.9% NaCl aqueous solution). The counter electrode was a Pt foil and the reference electrode was a saturated calomel electrode (SCE). Solutions were prepared using analytical grade reagent and Millipore Milli-Q water (resistivity  $> 18 \text{ M}\Omega \text{ cm}$ ), and were not deaerated. Experiments were carried out at room temperature ( $25 \pm 1^\circ \text{C}$ ).

Corrosion potential and polarisation curve measurements were made with a EG&G PAR 273A potentiostat. Impedance measurements were carried out using a Solartron 1250 Frequency Response Analyser coupled to a Solartron 1286 Electrochemical Interface with a 10 mV rms perturbation in the frequency range 65 kHz to 0.1 Hz, five points per frequency decade, and controlled by ZPLOT software; simulations were performed with ZSIM CNLS software.

## 3. Results and discussion

### 3.1. Open circuit potential

All alloys show an increase in the open circuit potential immediately after immersion, indicative of the formation of a film of corrosion products on the surface, and corroborated by visual inspection. The variation of time is shown in Fig. 2 and demonstrates that the open circuit potential is significantly more positive in the case of the Ag–Hg alloy. Values of the open circuit potential after 3 h immersion are  $0.047 \text{ V}$  ( $\gamma_1\text{-Ag}_2\text{Hg}_3$ ),

Table 1  
Data obtained from polarisation curves

| Alloys                            | $E_{\text{cor}}$ (mV vs. SCE) |                | $I_{\text{cor}}$ ( $\mu\text{A cm}^{-2}$ ) |                | $R_p$ ( $\text{k}\Omega \text{cm}^2$ ) |                |
|-----------------------------------|-------------------------------|----------------|--|----------------|--|----------------|
|                                   | 10 min immersion              | 48 h immersion | 10 min immersion                           | 48 h immersion | 10 min immersion                       | 48 h immersion |
| $\gamma_1\text{-Ag}_2\text{Hg}_3$ | −89                           | −118           | 18.2                                       | 12.3           | 3.2                                    | 0.8            |
| $\gamma\text{-Ag}_3\text{Sn}$     | −430                          | −337           | 10.6                                       | 13.8           | 2.2                                    | 2.6            |
| $\gamma_2\text{-Sn}_7\text{Hg}$   | −538                          | −526           | 1.6  | 40.6           | 14.3                                   | 12.6           |

−0.405 V ( $\gamma\text{-Ag}_3\text{Sn}$ ) and −0.509 V versus SCE ( $\gamma_2\text{-Sn}_7\text{Hg}$ ). A stable value of the potential is reached within 20 min for Sn–Hg, then being almost invariant, 30 min for Ag–Hg with a slight trend towards more positive values and after 3 h for Ag–Sn. The last of these is indicative of passivation and rupture of the surface films.

### 3.2. Polarisation curves

Potentiodynamic polarisation curves are shown in Fig. 3 recorded after 10 min and 48 h immersion, and data from these curves are summarised in Table 1. It should be noted that the corrosion potentials are more negative than the open circuit values, which can be ascribed to the applied potentials reducing the oxide film thickness. The relative rates of corrosion are brought into evidence in Fig. 4. These show clearly the inflection at −0.35 V for Sn–Hg and the regions within which passivation or partial passivation occur for the other two alloys.

The simplest variations of current with potential are those of the Sn–Hg system which show no evidence of any passive region. The high corrosion currents in the anodic region are due to mercury and tin dissolution.

For Ag–Sn there is evidence of a passivation process beginning at −0.2 V and extending to  $\sim 0.1$  V versus SCE when the layer begins to break down in the solution employed. Cyclic voltammetry (not shown) suggests that this region corresponds to the formation of tin oxide (Sn(IV) oxide) and silver begins to oxidise at +0.1 V. Oscillations in the current suggest the formation and dissolution of the oxide layer, probably due to the formation of oxy-chloro complexes. In particular, for Ag–Sn after a short immersion time, there is also evidence of passivation at −0.4 up to −0.3 V, probably due to the formation of Sn(II) oxide, which disappears at −0.3 V when the current rises again (Fig. 4 and cyclic voltammetry).

Regarding the Ag–Hg system, a passive layer begins to form at around 0.2 V when the current decreases sharply. The behaviour after short and long immersion times is qualitatively very similar.

Comparing all three alloys, calculated corrosion current densities ( $I_{\text{cor}}$ ) do not show large differences with time for  $\gamma\text{-Ag}_3\text{Sn}$  and  $\gamma_1\text{-Ag}_2\text{Hg}_3$ . However,  $\gamma_2\text{-Sn}_7\text{Hg}$  showed a large increase in  $I_{\text{cor}}$ , although the value of  $R_p$  remained similar after 48 h compared with after 10 min immersion. These results reflect the formation of an adherent film of corrosion products blocking the metallic surface (visible to the naked eye as a black film and composed of tin and mercury oxides), which is thicker for  $\gamma_2\text{-Sn}_7\text{Hg}$  than for the other alloys.

### 3.3. Electrochemical impedance

The impedance responses of  $\gamma_1\text{-Ag}_2\text{Hg}_3$  in 0.9% NaCl solution at applied potentials close to the corrosion potential were measured; two examples are shown in Fig. 5. The general form is that of a depressed semicircle caused by the influence of the rough surface. Equivalent circuit fitting involved using a parallel combination of a resistance,  $R_1$ , and a constant phase element (CPE), this substituting the capacitance of the interfacial region. The fitted values are shown in Table 2. The CPE values, which reach almost  $1 \text{ mF cm}^{-2}$ , become slightly smaller with increasing applied poten-

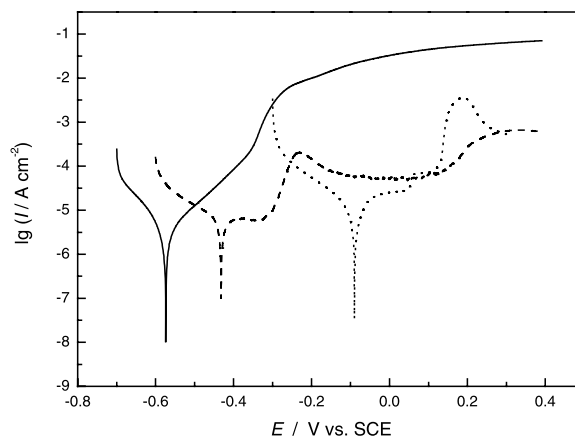


Fig. 4. Plot of  $\log I$  vs.  $E$  after 10 min immersion, data from Fig. 2: (—)  $\gamma_2\text{-Sn}_7\text{Hg}$ ; (---)  $\gamma\text{-Ag}_3\text{Sn}$ ; (···)  $\gamma_1\text{-Ag}_2\text{Hg}_3$ .

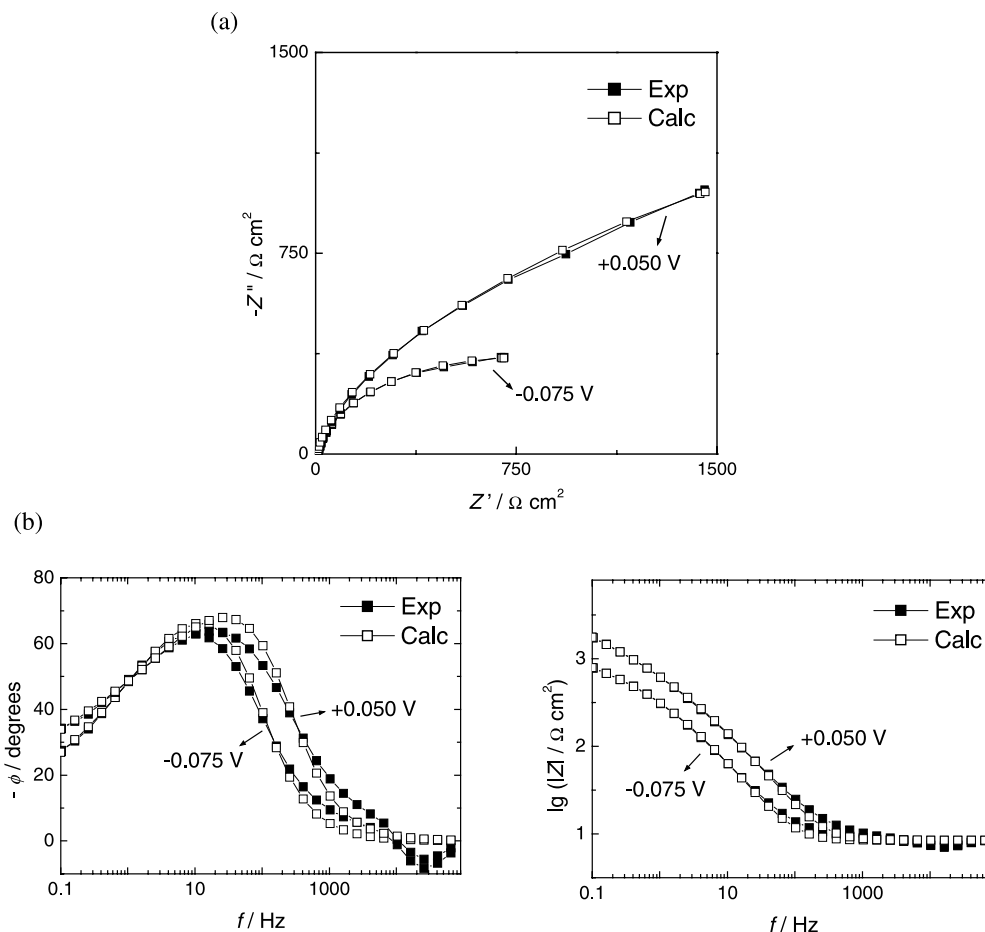


Fig. 5. Complex plane impedance plots for  $\gamma_1\text{-Ag}_2\text{Hg}_3$  after 10 min immersion in 0.9% NaCl: (a) complex plane; and (b) Bode format.

tial, as the values of  $R_1$ , of the order of  $\text{k}\Omega\text{ cm}^2$ , increase with increasing oxide thickness. Values of roughness are close to 0.5 for porous electrodes, as remarked above, and the high porosity is shown in the scanning electron micrograph in Fig. 6. The porosity, which appears systematic and happens in a similar way for the Sn–Hg samples, arises from the diffusion of mercury to the surface of the material during preparation, the effect of this being minimised by the application of a pressure of  $1.7 \times 10^5$  Pa.

Impedance responses of  $\gamma\text{-Ag}_3\text{Sn}$  in 0.9% NaCl solution at  $-0.4$  V versus SCE, close to the open circuit potential were obtained, exemplified in the complex plane plot in Fig. 7. The spectra were fitted with the same equivalent circuit as for  $\gamma_1\text{-Ag}_2\text{Hg}_3$ . Again, good agreement was found between the fitted values of  $R_1$  and the polarisation resistance values from the Tafel plots of Fig. 3.

As remarked above, unlike the other two phases studied, the surface of  $\gamma_2\text{-Sn}_7\text{Hg}$  readily oxidises natu-

rally to form oxides of tin and mercury. Thus the impedance spectra could be expected to be different, which is indeed the case. The impedance response of  $\gamma_2\text{-Sn}_7\text{Hg}$  at  $-0.55$  V versus SCE, close to the corrosion potential, is illustrated in Fig. 8, and can be adjusted with the same circuit. Values obtained are of a similar order of magnitude as for the other phases.

Table 2

Fitted values from impedance plots obtained at different applied potentials for  $\gamma_1\text{-Ag}_2\text{Hg}_3$

| $E$ (mV vs. SCE) | $R_1$ ( $\text{k}\Omega\text{ cm}^2$ ) | CPE ( $\text{mF cm}^{-2}$ ) |
|------------------|--|-----------------------------|
| -75              | 1.84                                   | 0.91                        |
| -50              | 2.12                                   | 0.69                        |
| -25              | 3.51                                   | 0.59                        |
| 0                | 6.70                                   | 0.55                        |
| 25               | 6.43                                   | 0.52                        |
| 50               | 6.75                                   | 0.52                        |

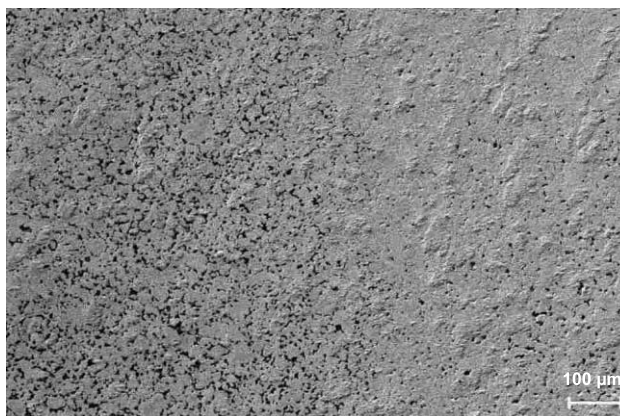


Fig. 6. Scanning electron micrograph of  $\gamma_1$ -Ag<sub>2</sub>Hg<sub>3</sub> alloy; the dimension bar represents 100  $\mu$ m.

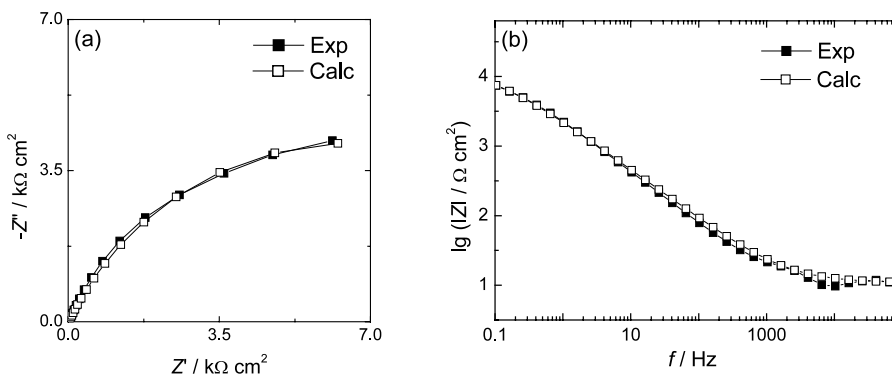


Fig. 7. Impedance spectra from  $\gamma$ -Ag<sub>3</sub>Sn sample after 10 min immersion in 0.9% NaCl: (a) complex plane; and (b) Bode format. Fitted values from equivalent circuit are  $CPE = 0.112 \text{ mF cm}^{-2}$ ,  $R_1 = 13.1 \text{ k}\Omega \text{ cm}^2$ ,  $\alpha = 0.72$ .

Nevertheless, on increasing the potential changes in the behaviour can be observed. From  $-0.3 \text{ V}$ , which corresponds to the inflection point in the curve of Fig. 4 where the current significantly increases, and at more positive values, there is the appearance of two time

constants and pseudo-inductive behaviour at low frequency. The currents at this point are significantly larger than for the other alloys which undergo passivation. A detailed study of this behaviour is being undertaken and will be reported later. Such inductive type

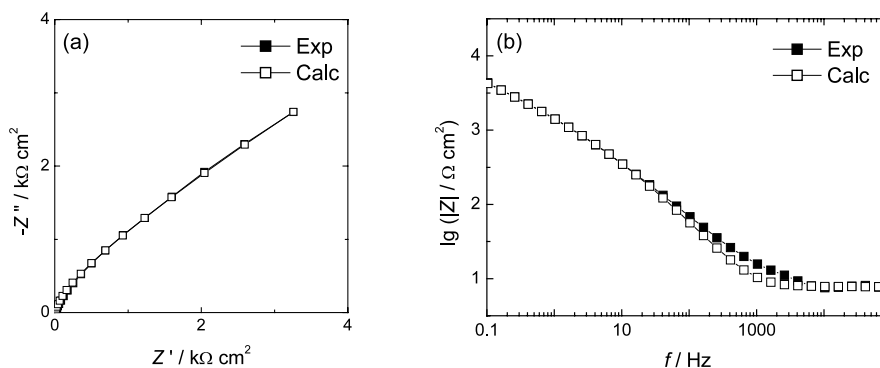


Fig. 8. Impedance spectra from  $\gamma_2$ -Sn<sub>7</sub>Hg sample after 10 min immersion in 0.9% NaCl: (a) complex plane; and (b) Bode format. Fitted values from equivalent circuit are  $CPE = 0.236 \text{ mF cm}^{-2}$ ,  $R_1 = 15.3 \text{ k}\Omega \text{ cm}^2$ ,  $\alpha = 0.58$ .

responses have been observed for various systems undergoing corrosion. A possible mechanism is a diffusional process towards a partially blocked electrode surface, which enables the non-homogeneity of the corroding surface to be taken into account. Another possibility involves an electroactive species with an adsorbed intermediate [3,6,7].

Comparing the impedance response of all three alloys after these relatively short immersion times only one time constant in the frequency range 65 kHz to 100 mHz is seen at potentials close to the open circuit. Since the phase angle maximum appears to be invariant with change in material, the same electrochemical process must occur for all the alloys at the values of potential studied. The effects of surface roughness are greatest for the  $\gamma_1$ -Ag<sub>2</sub>Hg<sub>3</sub> alloys and least for  $\gamma$ -Ag<sub>3</sub>Sn as corroborated by electron microscopy.

#### 3.4. Comparative remarks

Comparison of the mercury-containing phases shows noticeable differences, with the Sn–Hg system undergoing significantly greater corrosion except in the initial period. Once the oxide film has been removed, the Sn–Hg system undergoes much higher corrosion, in agreement with the literature assertions [3]. Comparison of the silver-containing phases shows that stability is conferred by the presence of Hg rather than Sn, which forms stronger chemical bonds. This is particularly evident from the much more positive corrosion potential values. The impedance response is in agreement with the above observations and a detailed study of its change with time will throw further light on the corrosion mechanism. A comprehensive surface analysis will also aid in this objective including X-ray photoelectron spectroscopy before and after corrosion, given its sensitivity to the first few atomic layers, together with ion bombardment to etch the surface and enable the recording of depth profiles.

#### 4. Conclusions

Open circuit potential measurements and polarisation curves show corrosion potentials most positive for  $\gamma_1$ -Ag<sub>2</sub>Hg<sub>3</sub>, followed by  $\gamma$ -Ag<sub>3</sub>Sn and then  $\gamma_2$ -Sn<sub>7</sub>Hg, reflecting the order of corrosion resistance after 48 h as measured by the corrosion currents. The electrochemical impedance data are in good agreement. The particular increase of the polarisation resistance calculated from impedance spectra with applied potential for  $\gamma_1$ -Ag<sub>2</sub>Hg<sub>3</sub> can be explained by variation of the resistance of the adherent corrosion film combined with high porosity.

Further characterisation of the amalgam phases with detailed examination of the time dependence of the impedance and surface properties is the object of further work being undertaken.

#### Acknowledgements

H.A.A. acknowledges a doctoral grant from FAPESP, process no. 97/12217-0.

#### References

- [1] H.A. Acciari, E.N. Codaro, A.C. Guastaldi, *Mater. Lett.* 36 (1998) 148.
- [2] G.R. Craig, *Restorative Dental Materials*, 9th ed., Mosby, St. Louis, USA, 1993, p. 289.
- [3] M. Marek, *The Corrosion of Dental Materials*, Academic Press, New York, 1983, p. 331.
- [4] J.L. Ferricane, T. Hanawa, T. Okabe, *J. Dent. Res.* 71 (1992) 1151.
- [5] M. Marek, *J. Dent. Res.* 72 (1993) 1315.
- [6] G. Palaghias, *Dent. Mater.* 1 (1985) 139.
- [7] G. Soh, C.L. Chew, A.S. Lee, T.S. Yeoh, *Quintessence Int.* 22 (1991) 225.
- [8] M. Marek, *Adv. Dent. Res.* 6 (1992) 100.
- [9] M.Z.A.M. Sulong, R.A. Aziz, *J. Prosthet. Dent.* 63 (1990) 342.
- [10] J.M. Meyer, J.N. Nally, *J. Dent. Res.* 54 (1975) 678.
- [11] B. Westerhoff, M. Darwish, R. Holze, *J. Appl. Electrochem.* 22 (1992) 1142.